Clays and Clay Minerals, Vol. 68, No. 1:38–49, 2020

LIQUID-PHASE XYLENE ADSORPTION IN UNARY, BINARY, AND TERNARY SOLUTE SYSTEMS USING RAW AND Ni^{2+} ION-EXCHANGED CLINOPTILOLITE: EXPERIMENTAL STUDY AND THERMODYNAMIC ASSESSMENT

Atefeh Salarvand[1] and Cavus Falamaki[1,2,3]*

[1]Chemical Engineering Department, Mahshahr Campus, Amirkabir University of Technology, Mahshahr 415, Iran
[2]Chemical Engineering Department, Amirkabir University of Technology, P.O. Box 15875-4413, Tehran, Iran
[3]Petrochemical Center of Excellence, Amirkabir University of Technology, P.O. Box 15875-4413, Tehran, Iran

Abstract—The adsorptive behavior of clinoptilolite (Cpt) zeolite in its raw and nickel-exchanged form towards *m*-xylene/*p*-xylene/ethylbenzene unary, binary, and ternary mixtures was investigated. The motivation behind the research was to elucidate whether Cpt in its raw or ion-exchanged form could exhibit distinctive selective adsorption behavior. The natural Cpt (Si/Al atomic ratio = 4.59) was ion-exchanged twice with 0.5 M $Ni(NO_3)_2$ solution at 80°C for 6 h. Adsorption experiments were done at 40°C, using a 4 vol.% solution of the aromatic materials in iso-octane. The maximum amount of the total specific adsorption capacity for binary solute systems was ~0.8 and ~2.0 mmol g^{-1} for the raw and ion-exchanged Cpt, respectively. For the ternary solute systems, unexpectedly, this capacity increased to ~2.0 and ~3.0 mmol g^{-1}, respectively. For binary mixtures, both forms of Cpt were selective for *p*-xylene. For ternary mixtures, both forms exhibited a clear selectivity for *m*-xylene but the Ni-exchanged Cpt was significantly higher over the concentration range studied. The unexpected increase in the adsorption capacity in ternary systems was attributed to the expulsion of tightly bound trace water molecules hindering the access of xylene molecules to the 10-member ring channels of the zeolite framework. Substitution of Mg^{2+} by Ni^{2+} in the 10-member ring channels enhanced the adsorption capacity by providing more space and stronger electrostatic interactions between the new cation and the polar *m*-xylene molecule.

Keywords—Adsorption · Clinoptilolite · Ion-exchange · *m*-xylene · Xylene isomers

INTRODUCTION

Natural zeolites are fine-grained geo-materials which, alongside clay minerals, are receiving increased interest in terms of environmentally sustainable agriculture (Manjaiah et al. 2019). In addition, the production of synthetic zeolites from clay minerals for use in the petrochemical and detergent industries (Takahashi & Nishimura 1968; Novembre et al. 2005) is increasing. The cutting-edge frontiers in the field of zeolites involve the production of hierarchical materials which show simultaneously micro-, meso- and macro-porosity (Feliczak-Guzik 2018; Wang et al. 2019). Clinoptilolite, an abundant natural zeolite, is becoming a potential competitor for synthetic zeolites in commercial separation and catalytic processes. The mineralogy and diagenesis of Cpt has been the subject of numerous research programs worldwide (Broxton et al. 1987; Altaner & Grim 1990; Noh 1998; Karakaya et al. 2015). It has attracted industrial interest for use in gas-separation processes for oxygen and nitrogen production from air (Ackley & Yang 1991a; Falamaki et al. 2004), separation of trace level N_2O from air (Centi et al. 2000), nitrogen separation from natural gas (Kouvelos et al. 2007; Liu et al. 2018; Kennedy et al. 2019), and H_2S separation from sour gas (Yaşyerli et al. 2002). Cpt has also been considered as an adsorbent for removing volatile organic compounds (VOCs), including xylene and styrene, from polluted air (Asilian et al. 2012). Catalytic processes include the dehydration of alcohols to ethers (Royaee et al. 2008), NO_x abatement by selective catalytic reduction of ammonia (Moreno-Tost et al. 2004) or hydrocarbons (Ghasemian et al. 2014a, 2014b; Dakdareh et al. 2018), and room-temperature (RT) liquid (aqueous) phase catalytic oxidation of soluble Fe^{2+} into insoluble Fe^{3+} (Azar & Falamaki 2012), among others. Liquid-phase separation processes consist mainly of separation of heavy metals by ion-exchange (Ni^{2+}, Pb^{2+}, Co^{2+}, Cu^{2+}, Fe^{2+}, Mn^{2+}, As^{3+} inter alia) in the aqueous phase, with great potential for the purification of acid mine drainage effluents (Motsi et al. 2011; Irannajad & Kamran Haghighi 2017). However, interest is also emerging in the removal of organic materials such as enzymes, humus, and living organisms like bacteria from waste and mine waters (Mamba et al. 2009; Ye et al. 2019). Recently, the potential application of modified forms of Cpt for deep desulfurization of liquid fuels (Mahmoudi & Falamaki 2016a, 2016b) and their dehydration has been reported (Favvas et al. 2016).

Selective adsorption of xylene isomers and ethylbenzene from their mixtures is an important task in the present petrochemical and specialty chemical industries. In particular, *p*-xylene selective adsorption using faujasite-type zeolites has been the subject of much research in the past (Minceva & Rodrigues 2004; Silva et al. 2012) and is the basis for simulated moving-bed adsorbers used currently in xylene isomerization plants throughout the world. On the other hand, *m*-xylene selective adsorption is also a sought-after industrial process in diverse sectors and a focus of recent research (Rasouli et al. 2012; Chen et al. 2018).

Clinoptilolite, as a natural zeolite, has many advantages for industrial and environmental applications. It is abundant and occurs in high-purity tuffs, it possesses inherent inorganic binders which impart suitable mechanical properties, and it is amenable to enhancement of its adsorption properties by

* E-mail address of corresponding author: c.falamaki@aut.ac.ir
DOI: 10.1007/s42860-019-00052-x

https://doi.org/10.1007/s42860-019-00052-x Published online by Cambridge University Press

applying simple and inexpensive physical/chemical treatments (Ackley et al. 2003; Farjoo et al. 2015).

To the knowledge of the present authors, the use of Cpt for liquid-phase adsorption separation processes in the petrochemical industries has been overlooked until now.

The purpose of the present study was, therefore, to investigate the potential use of high-purity Iranian Cpt and its ion-exchanged forms as a selective adsorbent to separate unary, binary, and ternary mixtures of *m*-xylene/*p*-xylene/ethylbenzene in the liquid phase. A further objective was to assess the thermodynamics of these multicomponent systems based on a theoretical approach developed previously (Hosseini & Falamaki 2015) which considers non-ideality of the adsorbed component in the solid phase.

EXPERIMENTAL

The raw Cpt used in this study was purchased from Afrand Tuska Co. (Tehran, Iran) with a purity of ~90 wt.% (impurity mainly SiO_2 polymorphs). Further information about this zeolite may be found elsewhere (Falamaki et al. 2004).

The raw Cpt was crushed to an average size of 120 μm, washed with 2 L of distilled water, and dried overnight at 120°C.

The Cpt was ion-exchanged with Ni^{2+} using the corresponding reagent-grade nitrate salt (Merck KGaA, Darmstadt, Germany). For this, 45 g of the dried raw Cpt was held in contact with a 0.5 M aqueous solution of $Ni(NO_3)_2$ at 80°C for 6 h under gentle agitation. The solid was then isolated and washed with >2 L of water. The whole process was repeated and the final zeolite was dried at 110°C for 24 h and labeled NiCpt.

Batch adsorption experiments were performed using reagent-grade *m*-xylene, *p*-xylene, and ethylbenzene (Loba Chemi, Mumbai, India). Iso-octane (Loba Chemi, Mumbai, India) was used as a solvent. For each experiment, 0.5 g of Cpt was weighed, placed in a glass vessel, heated in an electrical furnace at 300°C for 2 h, sealed with a septum cap and aluminum crimp ring (to avoid any water adsorption from the atmosphere), and allowed to cool to RT in a desiccator. Then, 5 mL of the organic solution containing solute(s)/solvent with predetermined concentrations was injected into the glass container through the septum. The latter was transferred to a shaker and shaken gently for 6 d at 40°C, at which point thermodynamic equilibrium was assumed, based on a previous liquid-phase study on BaX zeolite (SPX-3003, CECA, La Garenne-Colombes, France) which needed up to 6 d at 40°C to achieve nearly complete equilibrium (Hosseini & Falamaki 2015). Liquid-phase adsorption of xylene isomers and ethylbenzene, especially at low temperatures (near RT), is very difficult to perform because of the very low diffusion coefficients involved and the relatively viscous liquid.

Liquid-phase analysis was performed by ATR-FTIR analysis using a Thermo Nicolet Nexus 670 apparatus (San Diego, California, USA) equipped with a ZnSe crystal. For this purpose, several calibration curves were obtained and these revealed that the concentration detection error was <0.001%. Details of this analysis were given by Hosseini & Falamaki (2015). In brief, the amount of each organic material was related to the area of its representative peak appearing in the FTIR spectrum. The representative peaks were at 696 cm^{-1} for ethylbenzene, 690 cm^{-1} for *m*-xylene, 794 cm^{-1} for *p*-xylene, and 1363 cm^{-1} for iso-octane.

The cation concentration of the raw and modified Cpt was determined through X-ray fluorescence analysis using a Philips PW 1480 instrument (Philips, Amsterdam, Netherlands). Scanning electronc microscopy (SEM) analysis was performed using a Tescan VEGA3 (Brno, Czech Republic) instrument. Transmission electron microscopy (TEM) analysis was done using a Zeiss EM 10 C (Jena, Germany) instrument. X-ray diffraction (XRD) analysis was done using an INEL Equinox-3000 (Newfields, New Hampshire, USA) instrument with CuKα radiation and a germanium monochromator. Real-time detection was performed using a CPS120 detector with a radius of curvature of 250 mm and a detection angular range of 120°2θ and a FWHM equal to 0.08°2θ. *Match* software (version 1.11) was used for phase identifications from XRD patterns. A Quantachrome Nova 200 device (Boynton Beach, Florida, USA) was used for the measurement of the specific surface area of the raw and ion-exchanged Cpt.

RESULTS AND DISCUSSION

XRD analysis showed that the Cpt retained its crystallinity after the ion-exchange processes (Fig. 1). For NiCpt, the peak centered at 25.05°2θ was assigned to the $(\bar{3}12)$ planes of Cpt and increased in intensity upon ion-exchange with Ni^{2+}. The peak at ~70°2θ observed for NiCpt was probably due to SiO_2 polymorphs. Note that Cpt is a natural zeolite with a heterogeneous distribution of impurities; its general morphology prior to crushing and sizing has the appearance of anglular blocks (Fig. 2a). After crushing and sizing the crystallites have a flake-like morphology with a thickness of << 10 nm (Fig. 2b).

Analysis by X-ray fluorescence (XRF) of the Cpt and NiCpt (Table 1) revealed that the Si/Al molar ratio decreased from 5.96 to 5.52 as a result of the ion-exchange process. The ion-exchange of Cpt with just a single cation is known to be insufficient for complete substitution of the extra-framework cations with the new cations (Ackley & Yang 1991b; Falamaki et al. 2004), which explains the persistence of K^+, Ca^{2+}, and Mn^{2+} after Ni^{2+} exchange. Based on the XRF analysis, the number of the various cations present in a unit cell containing 413 *T* atoms (*T* = Al or Si) was calculated (Table 2), assuming that no extra-framework aluminum oxide existed in either Cpt or NiCpt. Based on these results, the ion-exchange process actually resulted in the near complete substitution of Mg^{2+} by Ni^{2+}. The substitution of Na^+ and K^+ by Ni^{2+} was minor. The exchange of Ca^{2+} with Ni^{2+} was significant; however, due to the large initial Ca^{2+} content in Cpt, the NiCpt zeolite still had a relatively large Ca^{2+} content.

The adsorption isotherms for the unary solute systems (Fig. 3a–c) revealed that NiCpt exhibited greater adsorption capacity for all the solutes under consideration than did Cpt, but Cpt

https://doi.org/10.1007/s42860-019-00052-x Published online by Cambridge University Press

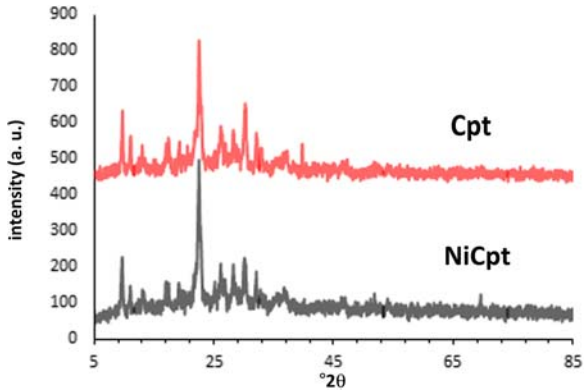


Fig. 1 XRD patterns of the raw and ion-exchanged zeolites

showed a substantially larger capacity to adsorb ethylbenzene and *p*-xylene compared to *m*-xylene. Such differences were much less pronounced in NiCpt, and the ethylbenzene and *p*-xylene isotherms were very similar. Interestingly, the maximum adsorption capacity of NiCpt was ~1 mmol/g^{-1}, which is similar to commercial BaX zeolite adsorbents such as SPX-3003 (CECA) (Hosseini & Falamaki 2015). The increase in adsorption capacity upon ion-exchange was attributed to the increase in specific surface area (from 50 to 120 m^2 g^{-1}) and the change in spatial conformation of the zeolite channel system. The latter factor will be discussed in more detail later.

The selectivities of Cpt and NiCpt for *m*-xylene and *p*-xylene in a binary solute system were obtained from the adsorption isotherms (Fig. 4a,b) and the corresponding separation factors, $\alpha_{i/j}$ (Fig. 4c,d). The relevant relationships are:

$$\alpha_{i/j} = \frac{z_i/z_j}{c_i/c_j}$$

z_i or z_j = fractional concentration of species *i* or *j* in the solid phase

c_i or c_j = concentration of species *i* or *j* in the liquid phase

Both Cpt and NiCpt exhibited a clear selectivity towards *p*-xylene over *m*-xylene (Fig. 4). For similar *m*-xylene adsorbate fractional concentrations, z_i , the separation factors $\alpha_{m-\text{xylene}/p-\text{xylene}}$ and $\alpha_{p-\text{xylene}/m-\text{xylene}}$ were approximately of the same magnitude regardless of which zeolite, Cpt or NiCpt, was tested. The main difference between the two zeolites, however, is the total specific adsorption capacity ($q_{m\text{-xylene}} + q_{p\text{-xylene}}$, q_i = specific adsorption capacity of species *i*) for similar liquid-phase concentrations of *m*-xylene or *p*-xylene. At high values of c_i, i.e. ~0.6 mol L^{-1}, the total adsorption capacity of NiCpt is more than twice that of Cpt.

Based on the adsorption isotherms for the ethylbenzene/*p*-xylene binary solute system (Fig. 5a,b) and the corresponding separation factor (Fig. 5c,d) calculations, neither Cpt nor NiCpt exhibited a significant separation factor for

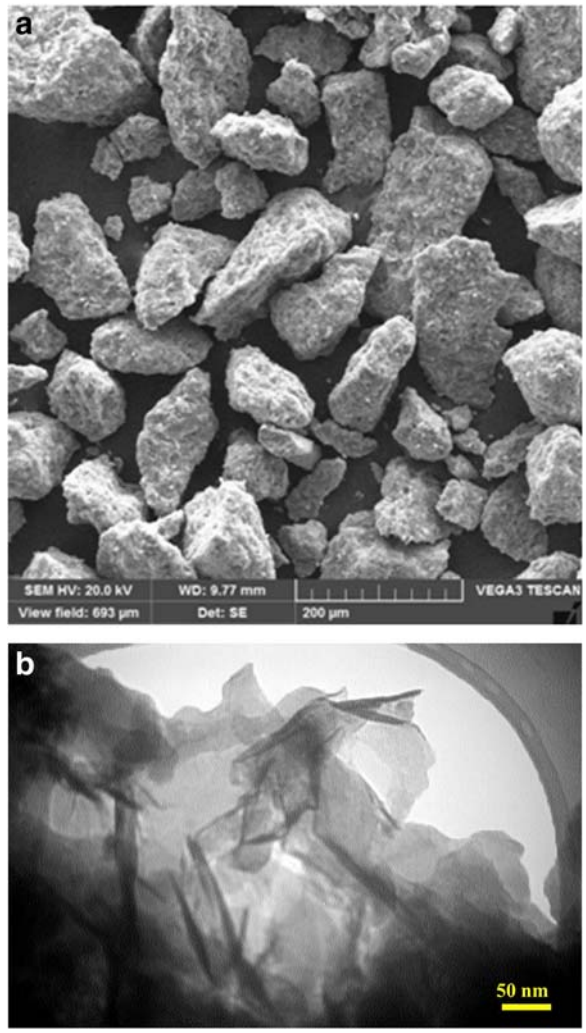


Fig. 2 (**a**) SEM image of the raw Cpt sample and (**b**) TEM image of a disintegrated Cpt sample

p-xylene (or ethylbenzene). Nonetheless, Cpt showed a slightly higher separation factor throughout the concentration range under study. Again, the total adsorption capacity of NiCpt was approximately twice that of Cpt.

At this stage, a better understanding of the interesting adsorption behavior of the binary solute systems is provided by referring to the thermodynamics of multi-solute adsorption of zeolites from liquids (Hosseini & Falamaki 2015). The basic relations used for the theoretical assessment of the adsorption data follow below.

In the case of multiple adsorbing solutes, the following equation holds (Hosseini & Falamaki 2015)

$$c_i^0 \, z_i \, \gamma_i = c_T \, x_i \qquad (1)$$

where c_i^0 is the liquid-phase concentration of single solute *i* at the real equilibrium spreading pressure; z_i, the adsorbed solute

https://doi.org/10.1007/s42860-019-00052-x Published online by Cambridge University Press

Table 1. XRF analysis as wt.% oxide of the Cpt and NiCpt zeolites. The error in the measurement of atom content is <1%

Zeolite	SiO_2	Al_2O_3	MgO	Na_2O	K_2O	CaO	TiO_2	MnO	NiO
CLP	69.30	8.90	0.84	0.95	2.17	2.89	0.22	0.21	0.00
NiCLP	61.44	8.51	0.02	0.82	2.83	2.48	0.24	0.38	3.66

i fraction in the zeolite; γ_i, the activity coefficient of solute *i* in the adsorbed state in the zeolite; c_T, the total solution concentration in the liquid-phase in equilibrium with the adsorbent; and x_i, the fraction of solute *i* in the liquid phase.

In Eq. 1, the liquid phase is considered to behave as an ideal solution. This is a satisfactory assumption, as the initial total liquid concentration before adsorption is low, near 4 vol.%. A key expression is then used for relating the spreading pressure to c_i^0 (Hosseini & Falamaki 2015):

$$S \cdot \pi\left(c_i^0\right) = \mathrm{R}T\int_0^{c_i^0} \frac{q\left(c_i^0\right)}{c_i^0} \quad dc_i^0 \tag{2}$$

where *S* stands for the zeolite specific surface area; $\pi\left(c_i^0\right)$, the spreading pressure corresponding to a single solute concentration of c_i^0; and $q\left(c_i^0\right)$, the invariant adsorption capacity of solute *i* at the spreading pressure of $\pi\left(c_i^0\right)$ and temperature *T*. R is the gas constant, i.e. 8.3145 J mol.$^{-1}$ K^{-1}.

The Gibbs-Duhem-Margules law has been used for binary solute systems as below:

$$\gamma_1 = \mathrm{A}\, z_2^2 \tag{3}$$

$$\gamma_2 = \mathrm{A}\, z_1^2 \tag{4}$$

where A is a constant (at constant temperature).

In the case of ternary solute systems, the consistency of the Gibbs-Duhem law is guaranteed using the geometric type model of Pelton (2001) as:

$$\gamma_1 = \mathrm{A}(z_2 - z_1 z_2) + \mathrm{B}(z_3 - z_1 z_3) - \mathrm{C}(z_2 z_3) \tag{5}$$

$$\gamma_2 = \mathrm{A}(z_1 - z_1 z_2) - \mathrm{B}(z_1 z_3) + \mathrm{C}(z_3 - z_2 z_3) \tag{6}$$

$$\gamma_3 = -\mathrm{A}(z_1 z_2) + \mathrm{B}(z_1 - z_1 z_3) + \mathrm{C}(z_2 - z_2 z_3) \tag{7}$$

The spreading pressure of each solute *i* is calculated through Eq. 2 using the corresponding unary solute *i* isotherm (Fig. 4a–c). Next, the activity coefficient is calculated by Eq. 1 and implementing the Gibbs-Duhem law using Eqs. 3–4 for the binary and Eqs. 5–7 for the ternary solute system.

The solid-phase adsorbate activity coefficients for the *m*-xylene/*p*-xylene and ethylbenzene/*p*-xylene binary solute systems using Cpt and NiCpt as adsorbents were also calculated (Fig. 6). Considering first the *m*-xylene/*p*-xylene system (Fig. 6a,b), for both Cpt and NiCpt adsorbents, the activity coefficient for *p*-xylene in the adsorbed state was near 1 (ideal state). On the other hand, the activity coefficient of *m*-xylene in the adsorbed state showed an increasing deviation from ideality as its fractional concentration in the solid phase decreased.

This may be interpreted as the adsorbed *p*-xylene molecules interacting much less with the inner surfaces of the zeolite channels and/or with other adsorbed molecules than do *m*-xylene molecules. In addition, the aforementioned interaction of *m*-xylene with its surrounding atoms/molecules is less pronounced in the case of NiCpt than with Cpt (Fig. 6a,b). In other words, NiCpt provides a more favorable adsorption state for *m*-xylene than *p*-xylene molecules in the liquid concentration range studied. The greater interaction of *m*-xylene with the surface may be attributed partly to its greater dipole moment (0.35 D). The dipole moment of *p*-xylene is 0.0 D.

Considering the variation of species activities as a function of fractional loading of ethylbenzene ($z_{\text{ethylbenzene}}$) for the ethylbenzene/*p*-xylene binary solute system (Fig. 6c,d), the experimental data indicated that *p*-xylene and ethylbenzene follow a similar trend for $z_{\text{ethylbenzene}}$ values >0.3. Again, Cpt exhibited a larger deviation of the activity coefficient for both species from 1 toward larger values. In the case of NiCpt, however, the activity coefficients were mostly near 1 (but < 1). Based on these calculated activity coefficients, one may conclude that NiCpt provides a more comfortable adsorption environment for ethylbenzene and *p*-xylene species than does Cpt.

The adsorption behavior and corresponding thermodynamic assessment may be better explained by referring to the framework structure of clinoptilolite. Based on the pioneering works of Koyoma & Takeuchi (1977) and Ackley & Yang (1991b), a descriptive image of Cpt and NiCpt zeolites has been

Table 2. Number of various cations, Si/Al atomic ratio, total number of *T* atoms (*T* = Al or Si), and total number of atoms per unit cell based on XRF analysis considering 10 wt.% impurity as SiO_2 polymorphs. The unit cell drawn in Figs 7 and 11 contains 413 *T* atoms. For each zeolite, the total charge of the cations per unit cell equals half the number of Al atoms. No extra-framework aluminum atom is taken into consideration

Zeolite	Na	K	Mg	Ca	Mn	Ni	Al	Si	Si/Al	# *T* atoms	# cation atoms per unit cell
Cpt	8.0	12.0	10.9	26.9	1.5	0.0	59.4	353.6	5.96	413	29.7
NiCpt	6.4	9.4	0.2	21.3	2.5	23.6	63.3	349.7	5.52	413	31.7

https://doi.org/10.1007/s42860-019-00052-x Published online by Cambridge University Press

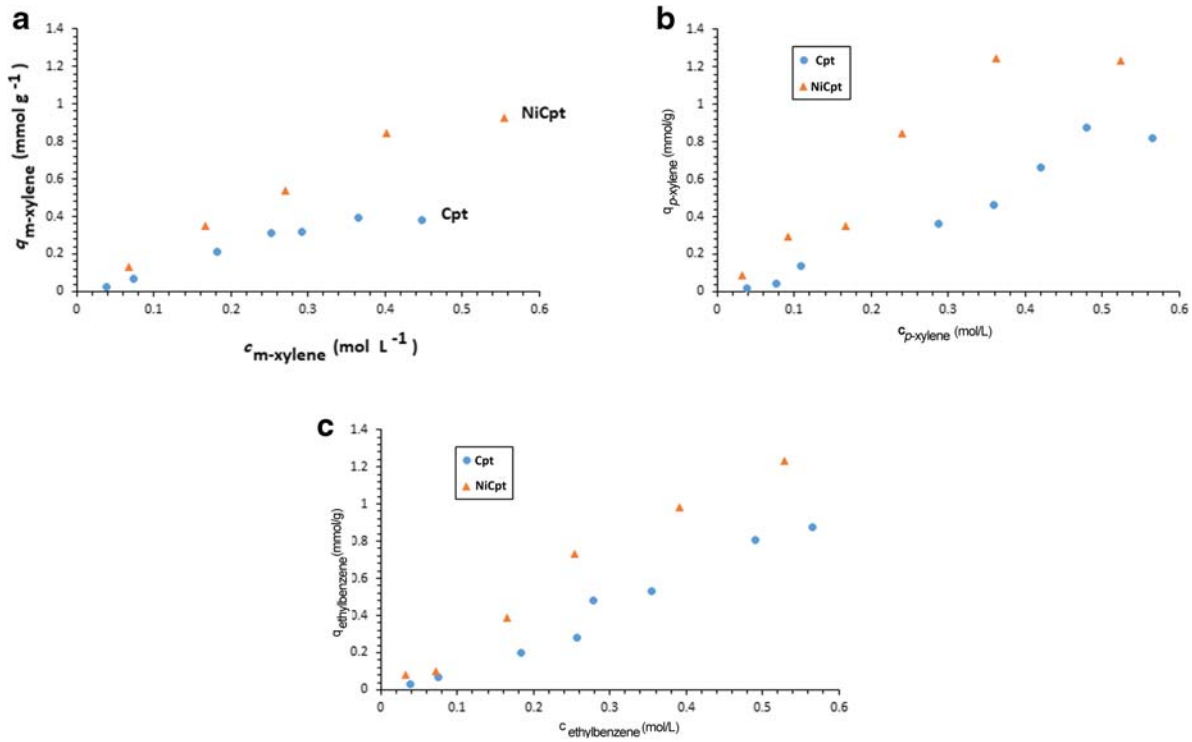


Fig. 3 Adsorptions isotherms of (**a**) *m*-xylene, (**b**) *p*-xylene, and (**c**) ethylbenzene from their unary solutions in iso-octane for Cpt and NiCpt adsorbents. The reproducibility error is ~1.5%

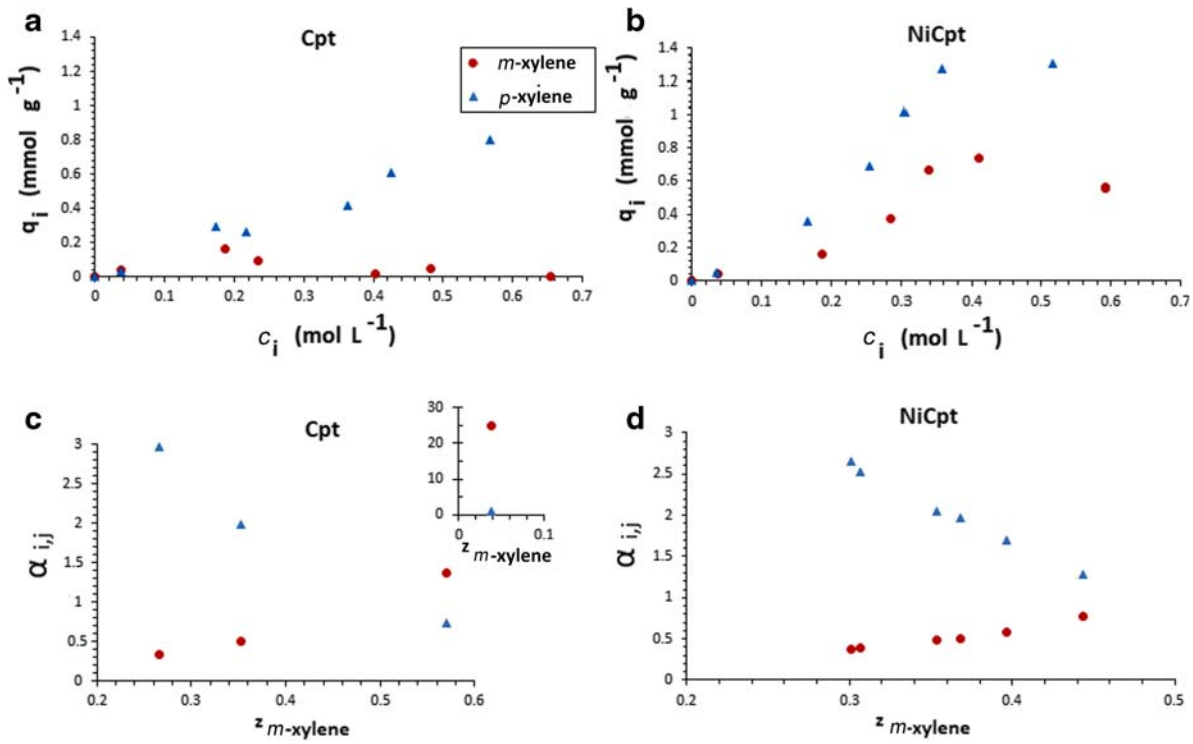


Fig. 4 *m*-xylene/*p*-xylene binary solute system: (**a**) specific adsorption (q_i) as a function of species concentration in the liquid phase (c_i) for Cpt, (**b**) specific adsorption (q_i) as a function of species concentration in the liquid phase (c_i) for NiCpt, (**c**) $\alpha_{i/j}$ for Cpt, and (**d**) $\alpha_{i/j}$ for NiCpt

https://doi.org/10.1007/s42860-019-00052-x Published online by Cambridge University Press

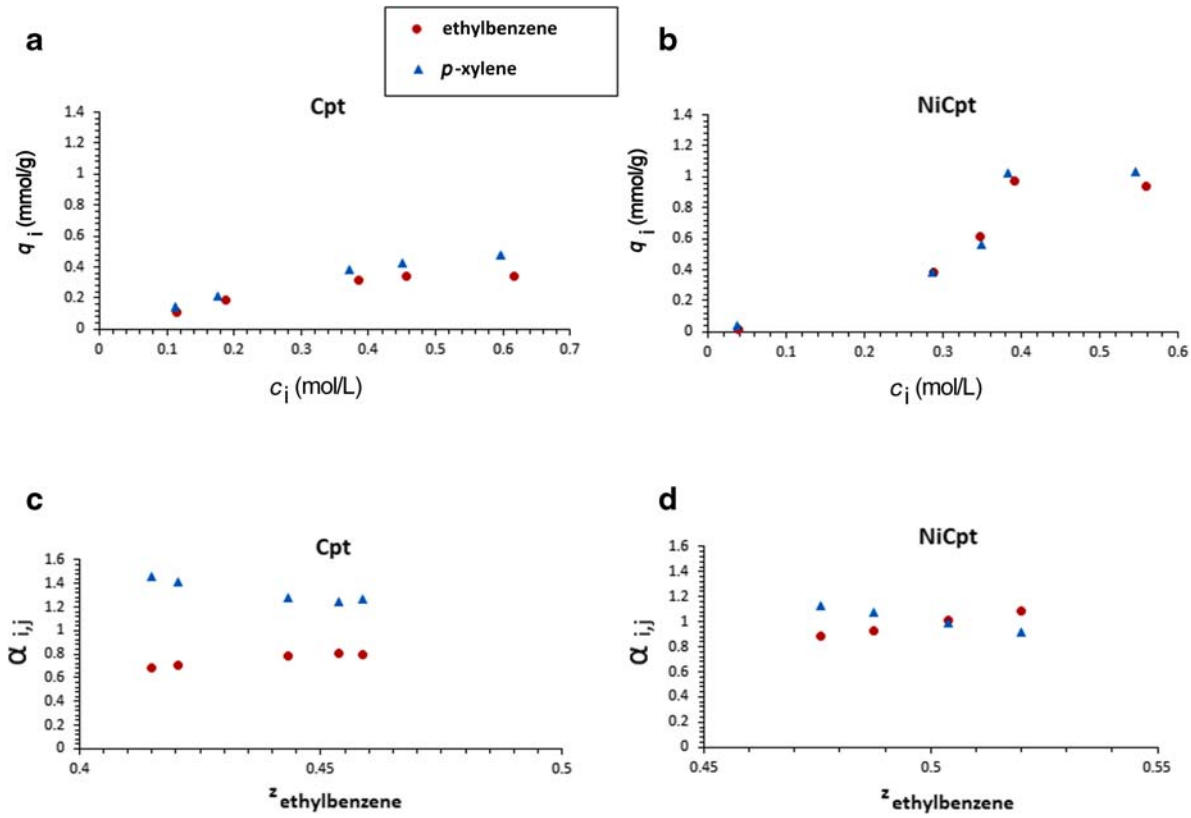


Fig. 5 Ethylbenzene/*p*-xylene binary solute system: (**a**) specific adsorption (q_i) as a function of species concentration in the liquid phase (c_i) for Cpt, (**b**) specific adsorption (q_i) as a function of species concentration in the liquid phase (c_i) for NiCpt, (**c**) α_{ij} for Cpt, and (**d**) α_{ij} for NiCpt

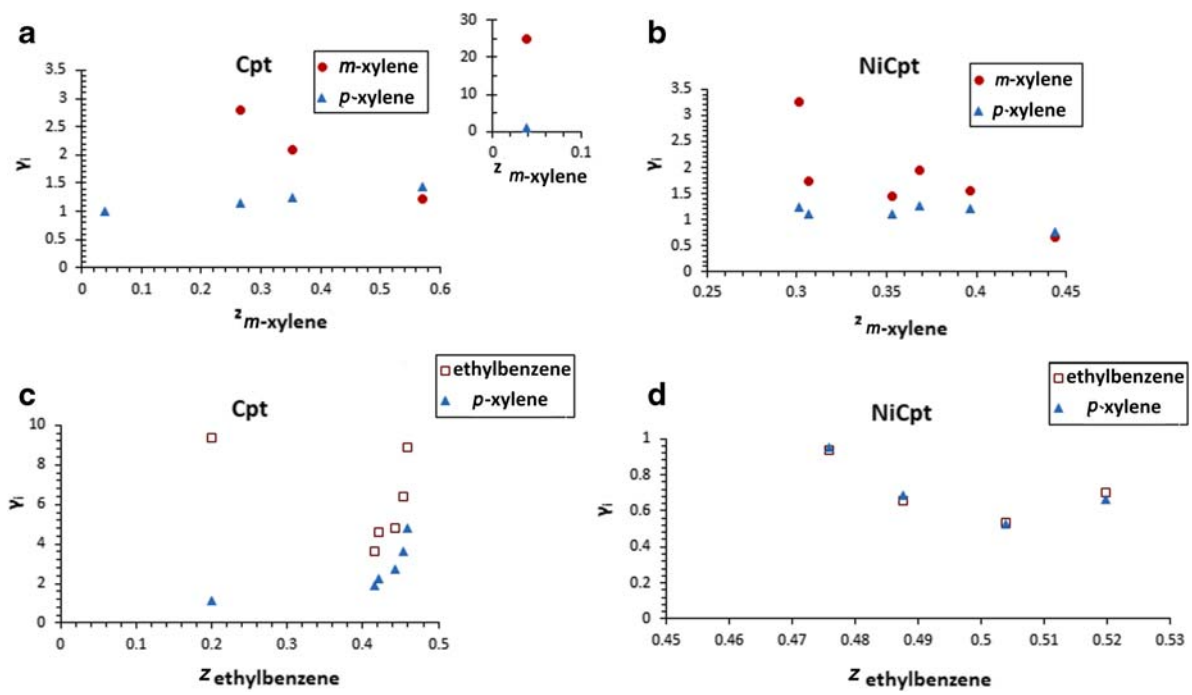


Fig. 6 Activity coefficients for the (**a**) *m*-xylene/*p*-xylene system for Cpt adsorbent, (**b**) *m*-xylene/*p*-xylene system for NiCpt adsorbent, (**c**) ethylbenzene/*p*-xylene system for Cpt adsorbent, and (**d**) ethylbenzene/*p*-xylene system for NiCpt adsorbent

https://doi.org/10.1007/s42860-019-00052-x Published online by Cambridge University Press

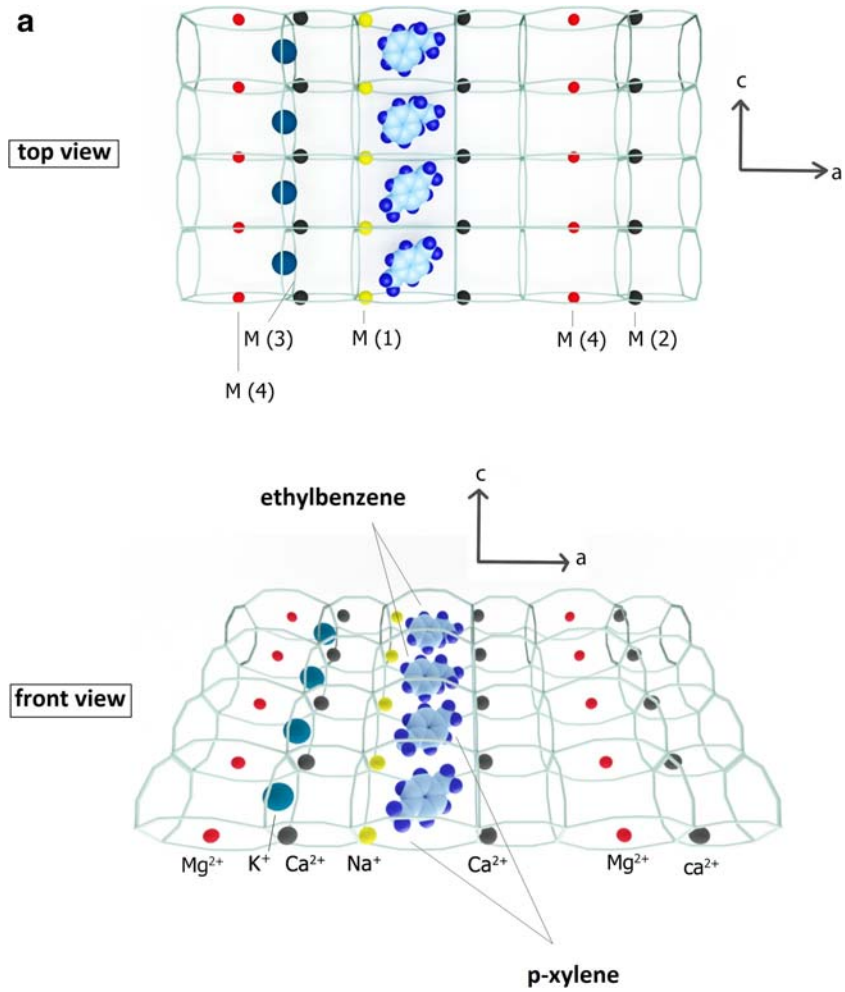


Fig. 7 (**a**) 3D framework structure of Cpt, (**b**) 3D framework structure of NiCpt. The number of the various cations is not exactly that of Table 2 (calculated), but is similar. In Fig. 7b the structures of the three organic molecules under study are depicted and the corresponding dipole moment indicated

envisaged (Fig. 7a,b). These figures show the cross-section of the zeolite in the *a*–*b* plane, where the periodic adjacency of the 10-member and 8-member ring channels has been depicted. In the same figure, the four different cation sites, labeled M(1) to M(4) by Ackley & Yang (1991b), are indicated. Recall that cation-occupied M(4) sites are completely inaccessible to xylene isomers and ethylbenzene. Based on the data summarized in Table 2, ion-exchange results in an almost complete substitution of Mg^{2+} cations by Ni^{2+} cations. On the other hand, the binary adsorption experiments showed that the adsorption capacity of NiCpt is almost double that of Cpt. Putting these two pieces of information together, the introduced Ni^{2+} cations obviously do not occupy M(4) type sites as do the parent Mg^{2+} cations. Instead, they may occupy M(1) sites. In addition, upon ion exchange with Ni^{2+} cations, ~25% of Na^{+} cations are substituted by smaller Ni^{2+} cations in one of the 10-member ring channels. Recall that two Na^{+} cations are substituted by one Ni^{2+} cation.

Putting all these facts together leads to the result that the induced conformation change upon ion exchange creates substantially more open 10-member windows (maximum diameter 7.2 Å instead of 3.6 Å), allowing entrance of *m*-xylene (0.68 Å), *p*-xylene (0.58 Å), and ethylbenzene (0.60 Å) molecules. In the case of the raw Cpt, *m*-xylene cannot enter the channel due to geometric hindrance. All of this is illustrated graphically in Fig. 7a which deliberately shows the prohibited entrance of *m*-xylene into the 10-member ring channels containing Na^{+} cations.

The ternary solutes system was considered next. Figures 8a and b show the specific adsorption capacity for each species as a sole function of *p*-xylene concentration in the liquid phase for Cpt and NiCpt adsorbents, respectively. The corresponding separation factors (Table 3) revealed, surprisingly, that both Cpt and NiCpt zeolites were selective for *m*-xylene over most of the *p*-xylene concentration range studied. However, a clear difference existed between the adsorptive behaviors of the two adsorbents. The specific adsorption capacity for *m*-xylene decreased steadily with increasing *p*-xylene for Cpt (Fig. 8), and eventually the zeolite became more selective toward

https://doi.org/10.1007/s42860-019-00052-x Published online by Cambridge University Press

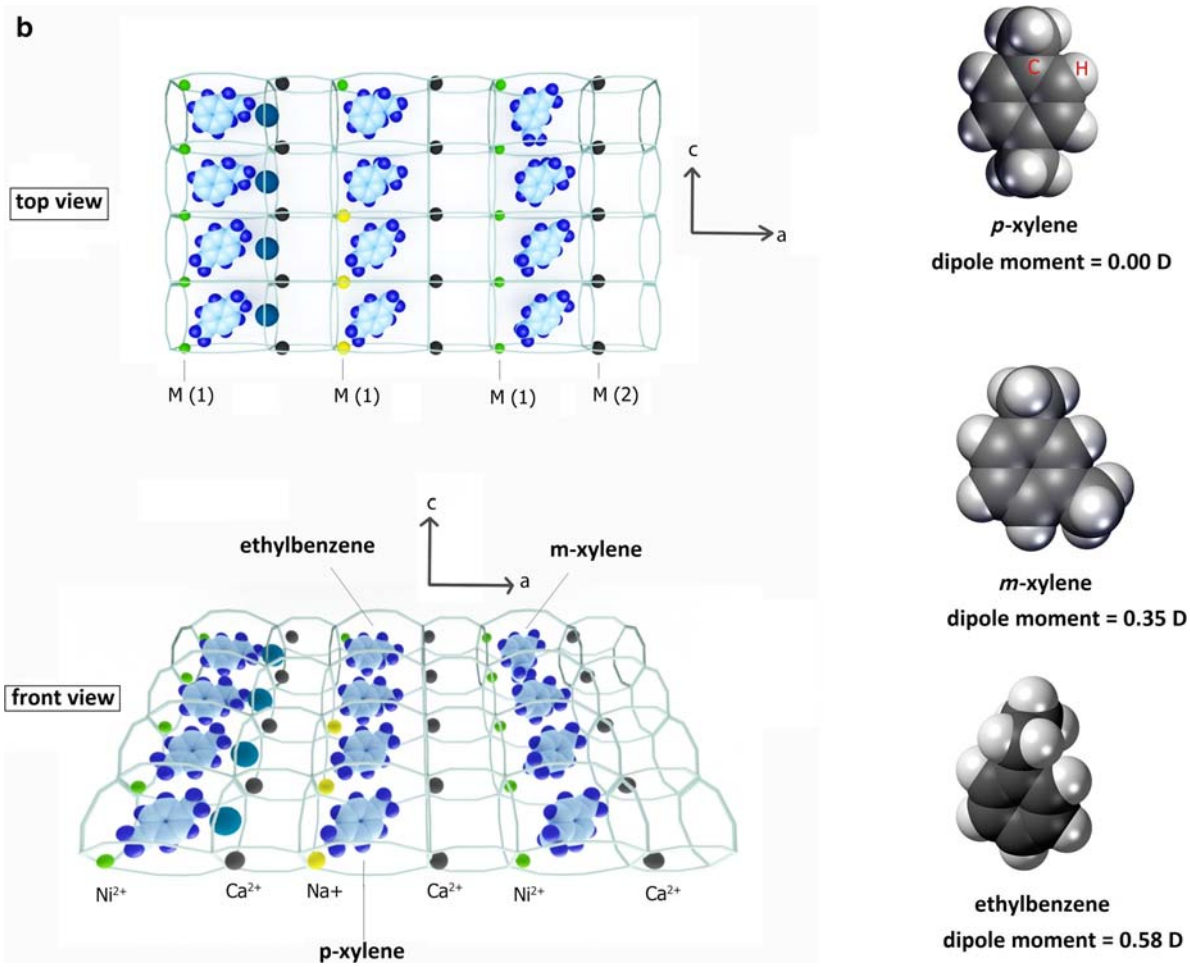


Fig. 7 (continued)

p-xylene at high concentrations ($c_{p\text{-xylene}}$ = 0.4 mole L^{-1}). This was not the case for NiCpt, however. The latter remained selective for *m*-xylene throughout the concentration range investigated. Recall that both zeolites showed selectivity for *p*-xylene in the binary solute systems.

With respect to the ternary solutes systems, another point needs to be highlighted. The maximum amount of the total specific adsorption capacity for the binary solute systems was ~0.8 and 2.0 mmol g^{-1} for Cpt and NiCpt, respectively (Figs. 5 and 6). The maximum total specific adsorption capacity for ternary solute systems increased to ~2.0 and 3.0 mmol g^{-1} for Cpt and NiCpt, respectively (Fig. 9). This is anomalous behavior, not reported previously. Cpt exhibited its maximum capacity even at the smallest *p*-xylene concentration of 0.06 mol L^{-1}, while the

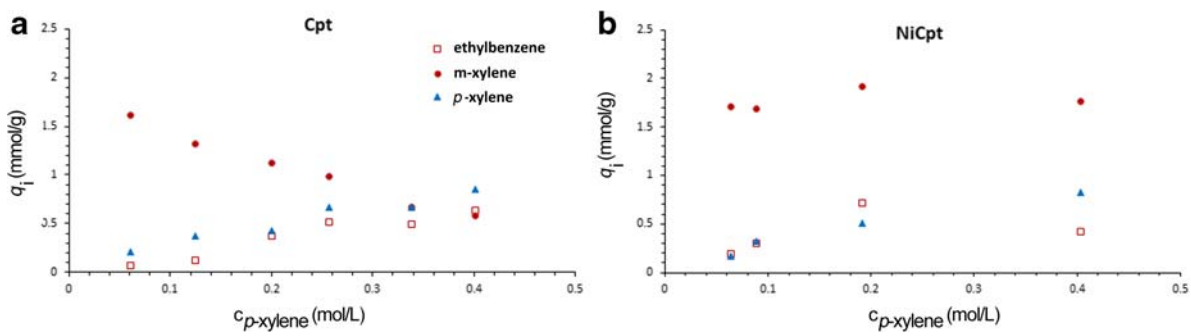


Fig. 8 Adsorption isotherms for ternary solute systems using (**a**) Cpt, and (**b**) NiCpt adsorbents

https://doi.org/10.1007/s42860-019-00052-x Published online by Cambridge University Press

Table 3. Separation factors for the ternary experiments. EB stands for ethylbenzene

Number of experiment	Zeolite	$c_{m\text{-xylene}}$ (mol/L)	$c_{p\text{-xylene}}$ (mol/L)	c_{EB} (mol/L)	α *m*-xylene/EB	α *p*-xylene/EB	α *m*-xylene/*p*-xylene
1	Cpt	≈ 0.00	0.06	0.06	NA	3.42	NA
2	Cpt	0.03	0.13	0.12	44.89	3.00	14.98
3	Cpt	0.13	0.21	0.20	4.84	1.21	4.01
4	Cpt	0.23	0.28	0.26	2.35	1.40	1.67
5	Cpt	0.34	0.36	0.34	1.45	1.43	1.01
6	Cpt	0.43	0.43	0.40	0.91	1.42	0.64
7	NiCpt	≈ 0.00	0.06	0.06	NA	0.90	NA
8	NiCpt	≈ 0.00	0.09	0.09	NA	1.14	NA
9	NiCpt	0.05	0.19	0.17	9.14	0.65	14.01
10	NiCpt	0.31	0.40	0.45	6.01	2.14	2.80

same was attained at higher *p*-xylene concentrations for NiCpt. In accordance with the early work of Falamaki et al. (2004), the pore volume of the Cpt zeolite used in the present study has been calculated to be 0.25 $cm^3\ g^{-1}$, based on the Dubinin-Astakhov semi-theoretical model (Ackley & Yang 1991b). Ackley & Yang (1991a) reported a greater value of 0.28 $cm^3\ g^{-1}$ for their clinoptilolite (of different Si/Al ratio compared to the Cpt of the present study). Considering a liquid density of 0.86 g cm^{-3} for the xylene isomers/ethylbenzene mixtures in the zeolite micro-channels, the maximum total adsorption capacity for Cpt was calculated to be 2.02 mmol g^{-1}. This agrees with the experimental result for Cpt. Accordingly, the pore volume of NiCpt should be > 2.02 mmol g^{-1} due to the substitution of Mg^{2+} by Ni^{2+} cations. The question now is why the maximum capacity is exhibited in the ternary systems and not in the binary systems.

The change in the total adsorption capacity and isomer adsorption selectivity for both Cpt and NiCpt when shifting from binary to ternary systems needs a rational theoretical explanation. To this end, the ATR-FTIR patterns of the final liquid-phase solution with the largest *p*-xylene concentration after reaching equilibrium were considered (Fig. 10). The ATR-FTIR patterns of the pure *m*-xylene, *p*-xylene, ethylbenzene, and iso-octane species were included for comparison.

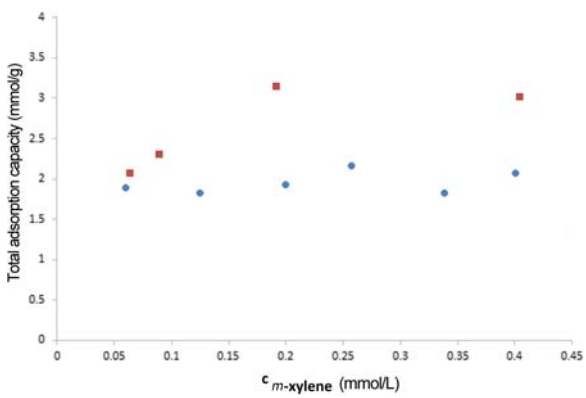


Fig. 9 Total adsorption capacity for ternary mixtures using zeolites Cpt and NiCpt as a function of *p*-xylene concentration in the liquid phase

Considering the ternary solution in contact with NiCpt zeolite, based on the peak identifications indicated in Fig. 10, no extra organic material could be detected. Although not shown for the sake of clarity, no measurable peak existed in the 3000–3900 cm^{-1} wavenumber range, which demonstrated the absence of detectable water molecules in the final solution. Remember that the detection error for the xylene isomers, ethylbenzene, and iso-octane species in the ATR-FTIR experiments was ~0.001%. The detection limit for any organic/inorganic (water) molecules is unknown, but is presumably not more than a few orders of magnitude higher. Based on this short introduction, the authors of the present work exclude the possibility of the egression of residual organic bulky molecules from Cpt and NiCpt upon contact with ternary solutions at 40°C for long periods (6 days). The egression of trace residual water molecules is possible, but not detectable.

Summing up, the substantial increase in total adsorption capacity of Cpt and NiCpt cannot be due to the formation of large void volumes created by the abandonment of bulky residual molecules residing within the 3D channel system. Instead, the phenomenon may be due to the elimination of geometric barriers to the free movement of xylene/ethylbenzene molecules. At this stage, a review of the different kinds of water molecules associated with the clinoptilolite is necessary.

The thermal dehydration of clinoptilolite has been the subject of numerous studies in the past and a wealth of knowledge about the types of water molecules associated with its framework at different temperatures is available. The various types of water molecules are generally classified as external, loosely bound, or tightly bound (Knowlton et al. 1981). The ratio of loosely bound to tightly bound is usually > 2. External and loosely bound water leaves the zeolite by heat treatment in the temperature range 50–200°C, while the tightly bound leaves over a wide temperature range (200–700°C) (Knowlton et al. 1981). Heat treatment at 300°C under atmospheric air and 2 h time period leaves behind a water content of <1 wt.% of tightly bound water molecules in the clinoptilolite in the present study. This small water content, however, seems to be very effective in reducing the total adsorption capacity for organic material. Due to the relatively large size of the xylene/

https://doi.org/10.1007/s42860-019-00052-x Published online by Cambridge University Press

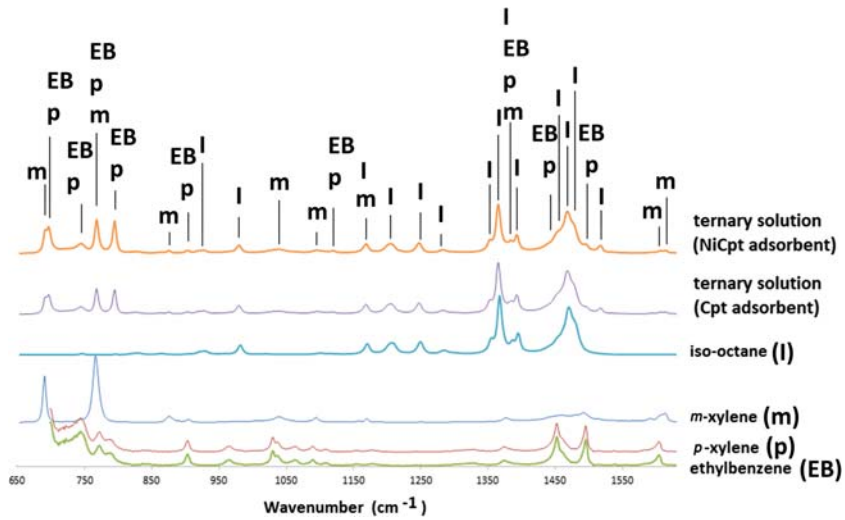


Fig. 10 ATR-FTIR patterns of various liquid-phase solutions. In the case of ternary mixtures, the solutions are those used with the largest organic-material concentration and after reaching thermodynamic equilibrium

ethylbenzene molecules, trace amounts of water molecules are able to tighten their path within the *a* direction of the 8-member ring channels, reducing the adsorption capacity (Fig. 11a). The point is why does the zeolite attain its maximum adsorption capacity in the presence of ternary solutions? The reason lies in the fact that the simultaneous presence of *m*-xylene, *p*-xylene, and ethylbenzene in the solid phase is able to push the tightly bound water molecules out of the crossing points between the *a* direction 8-member ring channels and the *c* direction 10-member ring channels in which Ni^{2+} cations are present (Fig. 11a,b). The simultaneous presence of water and Ni^{2+} at these points does not allow the presence of any xylene or ethylbenzene

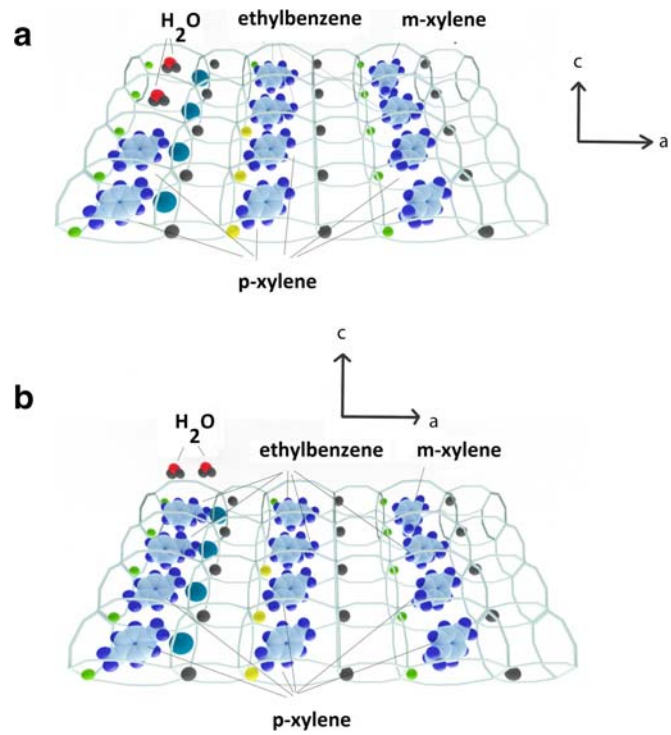


Fig. 11 (**a**) 3D framework structure of NiCpt before the egression of trace water molecules, and (**b**) 3D framework structure of NiCpt after contact with *m*-xylene/*p*-xylene/ethylbenzene ternary solution. Water molecules are dislocated by the organic molecules

https://doi.org/10.1007/s42860-019-00052-x Published online by Cambridge University Press

molecules due to space limitations. This discovery, which is based on experimental evidence, opens the way for the high energy-consuming, high-temperature heat treatments to be replaced by simple contact with dilute xylene isomers/ethylbenzene ternary mixtures.

The enhanced *m*-xylene selectivity in the case of ternary mixtures is explained as follows: some previous arguments were that ternary solutions facilitated entrance of the xylene isomers/ethylbenzene molecules into the 10-member ring channels by expelling the trace water molecules residing there. Accordingly, more xylene isomers, and especially *m*-xylene, may reach the previously difficult to reach Ni^{2+} cations; *m*-xylene, having a dipole moment of ~0.35 D, may have strong electrostatic interactions with Ni^{2+} cations in the 10-member rings, previously unreachable in binary solute systems. *p*-xylene molecules, having a dipole moment of zero, are free from this feature. Ethylbenzene molecules are not only more polar than *m*-xylene molecules but are also smaller. Why *m*-xylene adsorption is preferred by the Cpt over ethylbenzene is not clear at this stage but may be due to their lower packing in the 10-member ring channels. Further insight into the electrostatic interaction/packing needs molecular simulation.

Thermodynamic assessment of the ternary solute systems according to Eqs. 1–2 and 5–7, based on the unary solute results, may be prone to error. This is due to the subtle changes in the adsorbent micro-environment with respect to the unary and binary solute systems after contact with the ternary solution. However, if the error is ignored as a first approximation, calculations show that the states of adsorbed *m*-xylene, *p*-xylene, and ethylbenzene do deviate significantly from ideality, both for Cpt and NiCpt. Nevertheless, the activity of *m*-xylene is <1, and that of *p*-xylene and ethylbenzene is >> 1 throughout the concentration ranges studied. This presumably shows that *m*-xylene interaction with the zeolite inner surface and with other molecules that are present (*m*-xylene included) differs strongly from that of *p*-xylene and ethylbenzene molecules.

CONCLUSIONS

Clinoptilolite zeolite may be used effectively for highly selective adsorptive separation of *m*-xylene from *m*-xylene/*p*-xylene/ethylbenzene mixtures, especially in the Ni^{2+}-exchanged form. The simultaneous presence of the xylene isomers/ethylbenzene compounds, even at dilute concentrations, is able to expel trace residual water molecules from the microporous channels, opening the way for complete filling of the micro voids with the organic molecules. This new finding may be applied in industries where complete or near complete egression of water molecules from the zeolite at minimal expense is desired.

More insight into the selective adsorption behavior of Cpt and NiCpt vs. *m*-xylene may be gained through future molecular modeling.

ACKNOWLEDGMENTS

Eng. Seyed Mohammad Seyed Hosseini is acknowledged for his assistance with the experiments and for scientific discussions.

Compliance with Ethical Standards

Conflict of Interest

On behalf of all authors, the corresponding author states that there is no conflict of interest.

REFERENCES

Ackley, M. W., Rege, S. U., & Saxena, H. (2003). Application of natural zeolites in the purification and separation of gases. *Microporous and Mesoporous Materials, 61*, 25–42. https://doi.org/10.1016/S1387-1811(03)00353-6.

Ackley, M. W., & Yang, R. T. (1991a). Adsorption characteristics of high-exchange clinoptilolites. *Industrial & Engineering Chemistry Research, 30*, 2523–2530. https://doi.org/10.1021/ie00060a004.

Ackley, M. W., & Yang, R. T. (1991b). Diffusion in ion-exchanged clinoptilolites. *AIChE Journal, 37*, 1645–1656. https://doi.org/10.1002/aic.690371107.

Altaner, S. P., & Grim, R. E. (1990). Mineralogy, chemistry, and diagenesis of tuffs in the Sucker Creek Formation (Miocene), eastern Oregon. *Clays and Clay Minerals, 38*, 561–572. https://doi.org/10.1346/ccmn.1990.0380601.

Asilian, H., Khavanin, A., Afzali, M., Dehestani, S., & Soleimanion, A. (2012). Removal of tyrene from air by natural and modified zeolite. *Health Scope, 1*, 7–11. https://doi.org/10.5812/jhs.4592.

Azar, R. P., & Falamaki, C. (2012). Removal of aqueous Fe^{2+} using MnO_2–clinoptilolite in a batch slurry reactor: Catalyst synthesis, characterization and modeling of catalytic behavior. *Journal of Industrial and Engineering Chemistry, 18*, 737–743. https://doi.org/10.1016/j.jiec.2011.11.112.

Broxton, D. E., Bish, D. L., & Warren, R. G. (1987). Distribution and chemistry of diagenetic minerals at Yucca Mountain, Nye County, Nevada. *Clays and Clay Minerals, 35*, 89–110. https://doi.org/10.1346/ccmn.1987.0350202.

Centi, G., Generali, P., dall'Olio, L., Perathoner, S., & Rak, Z. (2000). Removal of N_2O from industrial gaseous streams by selective adsorption over metal-exchanged zeolites. *Industrial & Engineering Chemistry Research, 39*, 131–137. https://doi.org/10.1021/ie990360z.

Chen, L., Zhu, D.-D., Ji, G.-J., Yuan, S., Qian, J.-F., He, M.-Y., Chen, Q., & Zhang, Z.-H. (2018). Efficient adsorption separation of xylene isomers using a facilely fabricated cyclodextrin-based metal–organic framework. *Journal of Chemical Technology & Biotechnology, 93*, 2898–2905. https://doi.org/10.1002/jctb.5644.

Dakdareh, A. M., Falamaki, C., & Ghasemian, N. (2018). Hydrothermally grown nano-manganese oxide on clinoptilolite for low-temperature propane-selective catalytic reduction of NO_x. *Journal of Nanoparticle Research, 20*, 309. https://doi.org/10.1007/s11051-018-4414-0.

Falamaki, C., Mohammadi, A., & Sohrabi, M. (2004). N_2 and O_2 adsorption properties of an Iranian clinoptilolite-rich tuff in the original and pre-exchanged forms. *Colloids and Surfaces A: Physicochemical and Engineering Aspects, 246*, 31–37. https://doi.org/10.1016/j.colsurfa.2004.07.015.

Farjoo, A., Sawada, J. A., & Kuznicki, S. M. (2015). Manipulation of the pore size of clinoptilolite for separation of ethane from ethylene. *Chemical Engineering Science, 138*, 685–688. https://doi.org/10.1016/j.ces.2015.08.044.

Favvas, E. P., Tsanaktsidis, C. G., Sapalidis, A. A., Tzilantonis, G. T., Papageorgiou, S. K., & Mitropoulos, A. C. (2016). Clinoptilolite, a natural zeolite material: Structural characterization and performance evaluation on its dehydration properties of hydrocarbon-based fuels. *Microporous and Mesoporous Materials, 225*, 385–391. https://doi.org/10.1016/j.micromeso.2016.01.021.

Feliczak-Guzik, A. (2018). Hierarchical zeolites: synthesis and catalytic properties. *Microporous and Mesoporous Materials, 259*, 33–45.

https://doi.org/10.1007/s42860-019-00052-x Published online by Cambridge University Press

Ghasemian, N., Falamaki, C., & Kalbasi, M. (2014a). Clinoptilolite zeolite as a potential catalyst for propane-SCR-NO_x: Performance investigation and kinetic analysis. *Chemical Engineering Journal, 236*, 464–470. https://doi.org/10.1016/j.cej.2013.10.061.

Ghasemian, N., Falamaki, C., Kalbasi, M., & Khosravi, M. (2014b). Enhancement of the catalytic performance of H-clinoptilolite in propane–SCR–NO_x process through controlled dealumination. *Chemical Engineering Journal, 252*, 112–119. https://doi.org/10.1016/j.cej.2014.04.039.

Hosseini, S. M. S., & Falamaki, C. (2015). An efficient algorithm for modeling the thermodynamics of multi-solute adsorption from liquids. *Fluid Phase Equilibria, 390*, 34–41. https://doi.org/10.1016/j.fluid.2015.01.016.

Irannajad, M., & Kamran Haghighi, H. (2017). Removal of Co^{2+}, Ni^{2+}, and Pb^{2+} by manganese oxide-coated zeolite: equilibrium, thermodynamics, and kinetics studies. *Clays and Clay Minerals, 65*, 52–62. https://doi.org/10.1346/ccmn.2016.064049.

Karakaya, M. Ç., Karakaya, N., & Yavuz, F. (2015). Geology and conditions of formation of the zeolite–bearing deposits southeast of Ankara (Central Turkey). *Clays and Clay Minerals, 63*, 85–109. https://doi.org/10.1346/ccmn.2015.0630202.

Kennedy, D. A., Khanafer, M., & Tezel, F. H. (2019). The effect of Ag^+ cations on the micropore properties of clinoptilolite and related adsorption separation of CH_4 and N_2 gases. *Microporous and Mesoporous Materials, 281*, 123–133. https://doi.org/10.1016/j.micromeso.2019.03.007.

Knowlton, G. D., White, T. R., & McKague, H. L. (1981). Thermal study of types of water associated with clinoptilolite. *Clays and Clay Minerals, 29*, 403–411. https://doi.org/10.1346/ccmn.1981.0290510.

Kouvelos, E., Kesore, K., Steriotis, T., Grigoropoulou, H., Bouloubasi, D., Theophilou, N., et al. (2007). High pressure N_2/CH_4 adsorption measurements in clinoptilolites. *Microporous and Mesoporous Materials, 99*, 106–111. https://doi.org/10.1016/j.micromeso.2006.07.036.

Koyama, K., & Takeuchi, Y. (1977). Clinoptilolite: the distribution of potassium atoms and its role in thermal stability. *Zeitschrift für Kristallographie – Crystalline Materials, 145*, 216–239.

Liu, X., Xie, W., Cui, X., Tan, Z., Cao, J., & Chen, Y. (2018). Clinoptilolite tailored to methane or nitrogen selectivity through different temperature treatment. *Chemical Physics Letters, 707*, 75–79. https://doi.org/10.1016/j.cplett.2018.07.045.

Mahmoudi, R., & Falamaki, C. (2016a). Ni^{2+}-ion-exchanged dealuminated clinoptilolite: A superior adsorbent for deep desulfurization. *Fuel, 173*, 277–284. https://doi.org/10.1016/j.fuel.2016.01.048.

Mahmoudi, R., & Falamaki, C. (2016b). A systematic study on the effect of desilication of clinoptilolite zeolite on its deep-desulfurization characteristics. *Nanochemistry Research, 1*, 205–213. https://doi.org/10.7508/ncr.2016.02.007.

Mamba, B. B., Dlamini, N. P., Nyembe, D. W., & Mulaba-Bafubiandi, A. F. (2009). Metal adsorption capabilities of clinoptilolite and selected strains of bacteria from mine water. *Physics and Chemistry of the Earth, Parts A/B/C, 34*, 830–840. https://doi.org/10.1016/j.pce.2009.07.010.

Manjaiah, K. M., Mukhopadhyay, R., Paul, R., Datta, S. C., Kumararaja, P., & Sarkar, B. (2019). Clay minerals and zeolites for environmentally sustainable agriculture. Pp. 309–329 in: *Modified Clay and Zeolite Nanocomposite Materials* (M. Mercurio, B. Sarkar, & A. Langella, editors). Elsevier, Amsterdam.

Minceva, M., & Rodrigues, A. E. (2004). Adsorption of xylenes on faujasite-type zeolite: Equilibrium and kinetics in batch adsorber. *Chemical Engineering Research and Design, 82*, 667–681. https://doi.org/10.1205/026387604323142739.

Moreno-Tost, R., Santamaría-González, J., Rodríguez-Castellón, E., Jiménez-López, A., Autié, M. A., González, E., et al. (2004). Selective catalytic reduction of nitric oxide by ammonia over Cu-exchanged Cuban natural zeolites. *Applied Catalysis B: Environmental, 50*, 279–288. https://doi.org/10.1016/j.apcatb.2004.01.019.

Motsi, T., Rowson, N. A., & Simmons, M. J. H. (2011). Kinetic studies of the removal of heavy metals from acid mine drainage by natural zeolite. *International Journal of Mineral Processing, 101*, 42–49. https://doi.org/10.1016/j.minpro.2011.07.004.

Noh, J. H. (1998). Geochemistry and paragenesis of heulandite cements in a Miocene marine fan-delta system of the Pohang Basin, Republic of Korea. *Clays and Clay Minerals, 46*, 204–214. https://doi.org/10.1346/ccmn.1998.0460211.

Novembre, D., Di Sabatino, B., & Gimeno, D. (2005). Synthesis of Na-A zeolite from 10 Å halloysite and a new crystallization kinetic model for the transformation of Na-A into HS zeolite. *Clays and Clay Minerals, 53*, 28–36. https://doi.org/10.1346/ccmn.2005.0530104.

Pelton, A. D. (2001). A general "geometric" thermodynamic model for multicomponent solutions. *Calphad, 25*, 319–328. https://doi.org/10.1016/S0364-5916(01)00052-9.

Rasouli, M., Yaghobi, N., Chitsazan, S., & Sayyar, M. H. (2012). Adsorptive separation of meta-xylene from C8 aromatics. *Chemical Engineering Research and Design, 90*, 1407–1415. https://doi.org/10.1016/j.cherd.2011.11.016.

Royaee, S. J., Falamaki, C., Sohrabi, M., & Ashraf Talesh, S. S. (2008). A new Langmuir–Hinshelwood mechanism for the methanol to dimethylether dehydration reaction over clinoptilolite-zeolite catalyst. *Applied Catalysis A: General, 338*, 114–120. https://doi.org/10.1016/j.apcata.2008.01.011.

Silva, M. S. P., Moreira, M. A., Ferreira, A. F. P., Santos, J. C., Silva, V. M. T. M., Sá Gomes, P., Minceva, M., Mota, J. P. B., & Rodrigues, A. E. (2012). Adsorbent Evaluation Based on Experimental Breakthrough Curves: Separation of *p*-Xylene from C8 Isomers. *Chemical Engineering & Technology, 35*, 1777–1785. https://doi.org/10.1002/ceat.201100672.

Takahashi, H., & Nishimura, Y. (1968). Formation of faujasite-like zeolite from halloysite. *Clays and Clay Minerals, 16*, 399–400. https://doi.org/10.1346/ccmn.1968.0160509.

Wang, C., Li, J., Wang, X., Yang, Z., & Huang, K. (2019). Preparation of a hierarchical pore zeolite with high-temperature calcination and acid-base leaching. *Clays and Clay Minerals*. https://doi.org/10.1007/s42860-019-00025-0.

Yaşyerli, S., Ar, İ., Doğu, G., & Doğu, T. (2002). Removal of hydrogen sulfide by clinoptilolite in a fixed bed adsorber. *Chemical Engineering and Processing: Process Intensification, 41*, 785–792. https://doi.org/10.1016/S0255-2701(02)00009-0.

Ye, J., Chen, X., Chen, C., & Bate, B. (2019). Emerging sustainable technologies for remediation of soils and groundwater in a municipal solid waste landfill site – A review. *Chemosphere, 227*, 681–702. https://doi.org/10.1016/j.chemosphere.2019.04.053.

(Received 5 October 2019; accepted 3 December 2019; AE: Jun Kawamata)

https://doi.org/10.1007/s42860-019-00052-x Published online by Cambridge University Press